Nanoscale

Accepted Manuscript

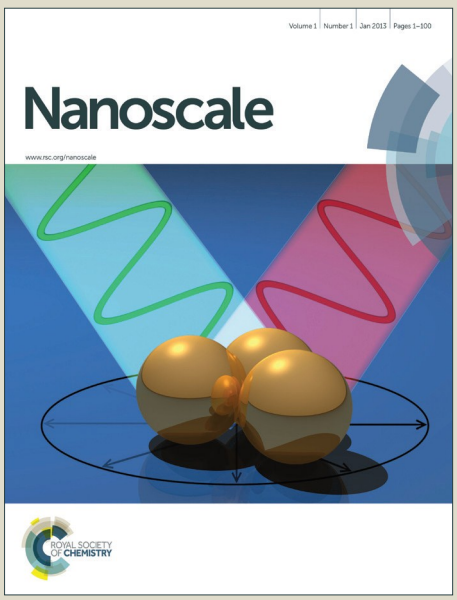

ROYAL SOCIETY OF CHEMISTRY

www.rsc.org/nanoscale

Nanoscale

ARTICLE

Cellulose Conjugated FITC-Labelled Mesoporous Silica Nanoparticles: Intracellular Accumulation and Stimuli Responsive Doxorubicin Release

Received 00th January 20xx,
Accepted 00th January 20xx

DOI: 10.1039/x0xx00000x

www.rsc.org/

Abdul Hakeem[b, d], Fouzia Zahid[b], Ruixue Duan [b], Muhammad Asif[b], Tianchi Zhang[b], Zhenyu Zhang[b], Yong Cheng[b], Xiaoding Lou [b], Fan Xia†[a, b& c]

Herein, we design a novel cellulose conjugated mesoporous silica nanoparticles (CLS-MSPs) based nanotherapeutics for stimuli responsive intracellular doxorubicin (DOX) delivery. DOX molecules are entrapped in pores of fabricated mesoporous silica nanoparticles (MSPs) while cellulose is used as encapsulating stuff through esterification on the outlet of pores of MSPs to avoid premature DOX release under physiological conditions. In *vitro* studies, stimuli responsive DOX release is successfully achieved from DOX loaded cellulose conjugated mesoporous silica nanoparticles (DOX/CLS-MSPs) by pH and cellulase triggers. Intracellular accumulation of DOX/CLS-MSPs in human liver cancer cells (HepG2 cells) is investigated through confocal microscope magnification. Cell viability of HepG2 cells is determined as the percentage of the cells incubated with DOX/CLS-MSPs with that of non-incubated cells through MTT assay.

Introduction

Cancer therapy is a gigantic challenge in current world. Numerous efforts have been made and different sort of techniques are being applied to control this dilemma such as radiation therapy, chemotherapy, immunotherapy, transplantation, hyperthermia, angiogenesis inhibitor therapy etc. Chemotherapeutic technique is considered as the premium option among all other therapeutic techniques in cancer treatment due to its feasibility in all type of cancers but it is still in early stages and even not successful to some extent yet. Certain mechanisms in cancer cells such as multiple drug resistance system (MDR), gene mutation, gene amplification and DNA damage repair etc. are the main reasons of cancer chemotherapy failure [1-2]. Beside these mechanisms, another key challenge in cancer chemotherapy is the toxicity of anticancer drugs on the normal cells because most forms of chemotherapeutic agents' target all rapidly dividing cells rather than targeting cancer cells specifically [3]. Though some degree of specificity comes from the inability of some cancer cells to repair DNA damage while normal cells can generally do repair DNA damage to some extent but in a very minor level. It is very key in chemotherapy to design certain anticancer drug delivery systems (ADDS) that deliver drug cargo on tumor targets selectively to avoid the toxicity drawback [4].

Nanocarriers are being employed as important strategies for drug delivery due to their capabilities of enhancing drug solubility, improving pharmacokinetics and preferentially their accumulation capability in cancer cells without being recognized by P-glycoprotein and enhanced permeability retention (EPR) effect [5-8]. Nanocarriers not only have more loading potency of the multiple agents, but even they accommodate their bio-distribution and plasma elimination, realizing an extremely simple dose optimization [9-11]. Among the other nanoparticles, silica nanoparticles based nanotherapeutics are rapidly building up and are being employed to solve several limitations of conventional drug delivery systems such as nonspecific biodistribution and targeting, lack of water solubility, poor bioavailability, and low therapeutic indices [12-14]. To improve the bio-distribution of cancer drugs, silica nanoparticles have been considered ideal contenders owing to their small size and surface uniqueness to enhance their circulation time in the bloodstream [15-17]. Silica nanoparticles are also capable to carry loaded active anticancer cargo molecules to cancer cells selectively by using the unique pathophysiology of tumors, such as their enhanced permeability and retention effect. Multifunctional and multiplex silica nanoparticles are now being actively investigated and are on the prospect as the next generation of nanoparticles to facilitate cancer treatment [18, 19]. Numerous silica nanoparticles based attempts have been reported so far to deliver the anticancer cargo to tumor cites [20-22]. Certain

[a] *Hubei Key Laboratory of Bioinorganic Chemistry and Materia Medica, Huazhong University of Science and Technology, Wuhan 430074, China*
[b] *School of Chemistry and Chemical Engineering, Huazhong University of Science and Technology, Wuhan 430074, China*
[c] Key Laboratory for Large-Format Battery Materials and System, Ministry of Education, School of Chemistry and Chemical Engineering, Huazhong University of Science and Technology, Wuhan 430074, China.
[d] Lasbela University of Agriculture, Water and Marine Sciences Uthal, Pakistan.
† Corresponding author, Email: xiafan@hust.edu.cn
Electronic Supplementary Information (ESI) available: [details of any supplementary information available should be included here]. See DOI: 10.1039/x0xx00000x

tumor cells conditions such as more acidified environment and more production of certain enzymes than normal cells provide an excellent opportunity to design the pH and enzyme responsive drug nanocarriers by conjugating with smart stimuli responsive materials. Many studies have been reported to respond the acidified lysosomal/endosomal microenvironment of cells but more improvement is highly demanded for controlled and targeted drug delivery in cancer chemotherapy particularly in real-time *in vivo* applications. In the best of our knowledge this is almost first attempt to respond the certain enzymes that are the part of cellular lysosomal/endosomal, lipases and sulfatases etc. All of these enzymes are active in cellular microenvironment. Lysosomes; membrane-bound vesicles, contain more than fifty digestive enzymes, such as glycosidases, proteases in lysosomal/endosomal acidified microenvironment and capable of breaking down of large biomolecules, such lipids, proteins, nucleic acids and carbohydrates.

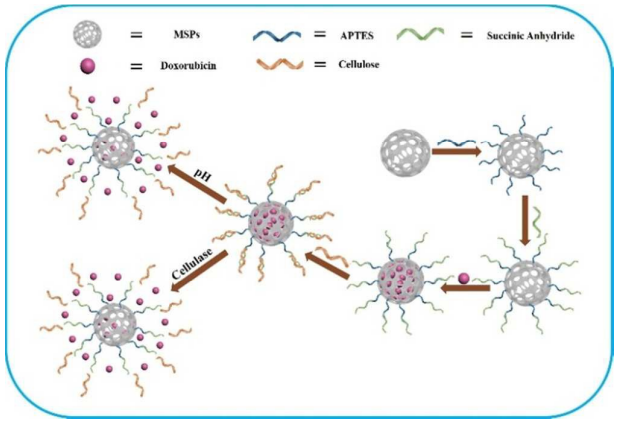

Figure 1: Flow chart of synthesis of MSPs based nanotherapeutics for doxorubicin delivery. NH_2 modification was created with APTES while COOH binding was carried out through succinic anhydride. Surface conjugation of cellulose was achieved by esterification between carboxylated MSPs and cellulose in presence of NHS/EDC. Dual responsive DOX release is achieved through pH and cellulase triggers.

Herein, we propose mesoporous silica nanoparticles based nanotherapeutic novel strategy that responds both glycosidase enzymes and acidified conditions of endosomal/lysosomal microenvironment. We synthesized porous MSPs and encapsulated anticancer drug doxorubicin inside their pores then sealed the outlets of pores with cellulose through esterification by surface conjugation (as shown in flow chart Figure 1). Cellulose surface conjugation of MSPs not only controls the drug release, even its cationic characteristic could also support the cellular internalization. Stimuli responsive DOX release is achieved by using cellulase glycosidase enzyme and pH triggers. Cellulase enzyme could digest the cellulose into small glucose units or cellodextrin units and ruptured the sealed pores of MSPs in order to release the encapsulated anticancer cargo (DOX) molecules while acid catalysed hydrolysis breaks the ester linkage and results in opening of pores of MSPs in order to release cargo. To the best of our knowledge, this is the first study about using cellulose for surface conjugation of MSPs to block the pore outlet in order to control the premature anticancer cargo release. Cellulose is straight chain polysaccharide in which D-glucosamine units condense with each other through β-(1-4) linkages. Cellulose polymer has many key advantages to employ as a gatekeeper due to its ester linkage making characteristics in the presence of -OH group, biodegradability, less toxicity, and the most important is its unabsorption in human stomach for control oral drug delivery. Its polymeric structure degrades into small glucose units in presence of glycosidase enzymes.

Results and Discussion

MSPs were synthesized by sol-gel method with well spherical shape and average diameter about 120 nm (TEM size). TEM images were taken to observe the porous structure of MSPs. Well-arranged two dimensional arrays of pores were observed throughout the surface of MSPs from TEM images that were large enough to load anticancer drug such as doxorubicin (DOX) molecules while small enough to close with cellulose (CLS) polymer molecules. For further surface modification, mesoporous silica nanoparticles were treated with 3-aminopropyltriethoxysilane (APTES) to create amino (NH_2) group and following with succinic anhydride (SA) to achieve COOH-MSPs nanoparticles (as shown in flow chart Figure 1). Surface modification with APTES and SA had no major effect on the average diameter and pore size of nanoparticles (as shown in table S1 in the supplementary information). Doxorubicin was selected as a model drug to investigate the drug loading and release behaviour of MSPs. Carboxylated mesoporous silica nanoparticles were soaked in DOX solution to absorb the drug molecules inside the pores for 48 h with constant stirring at ambient temperature to allow maximum DOX molecule penetration and then treated with acetate buffer solution (2 M, pH: 5) of EDC/NHS to activate carboxylic group of the surface then reacted with cellulose solution to create ester linkage between COOH group of MSPs surface and OH group of cellulose in order to entrap the DOX molecules inside by capping outlet of MSPs pores for controlled drug delivery.

Characterization: Synthesis and treatment process of MSPs nanoparticles was characterized through different instrumental techniques such as FTIR, TEM, XRD, TGA, DLS and N_2-adsorption/desorption. TEM images were taken by Techai G2 F20 S-Twin 200 KV High Resolution Transmission Electron Microscope. MSPs were dispersed in ethanol and spotted on the copper gird. TEM images of MSPs (Figure 2A) suggest that synthesized MSPs had large and well spread porous structure throughout the surface which was enough for loading anticancer cargo molecules. FTIR spectra were produced from Burker Vertex 70 FTIR Spectrometer. FTIR spectra (Figure 2B) confirm that surface modification of MSPs with APTES, succinic anhydride, and binding of cellulose through ester linkage was successfully achieved. FTIR spectra also confirm the step wise synthesis of MSPs, NH_2-MSPs, COOH-MSPs and CLS-MSPs. X-ray diffraction was recorded through Bruker D4 Powder X-ray

diffractometer using Cu Kα radiation. XRD pattern of MSPs (Figure 2C) suggests that fabricated MSPs were MCM-41 type mesoporous silica nanoparticles which are widely used for anticancer drug loading in the field of drug delivery.

Thermogravimetric Analysis (TGA) was performed by Perkin Elmer Pyris TG Analyser using nitrogen as an oxidant with continues heating from 30 °C to 796.84 °C at heating rate of 10 °C/min. TGA curves (Figure 2D) of MSPs, NH_2-MSPs, COOH-MSPs and CLS-MSPs further confirm that surface modification and esterification of MSPs with cellulose was carried out successfully. Weight loss of MSPs, NH_2-MSPs, COOH-MSPs and CLS-MSPs after heating up to 900 °C was 11.47, 14.12, 14.72 and 33.44% respectively. High weight loss by CLS-MSPs suggests that cellulose was conjugated on the surface of MSPs through ester linkage that was degraded at high temperature while MSPs was stable even up to 900 °C. The quantity of cellulose conjugated on the surface of nanoparticles was about 22 mg/100 mg of SiO_2. The amount of cellulose coated was also determined from weight difference of COOH-MSPs nanoparticles before and after esterification with cellulose that was about 23.53 mg/100 mg COOH-MSPs.

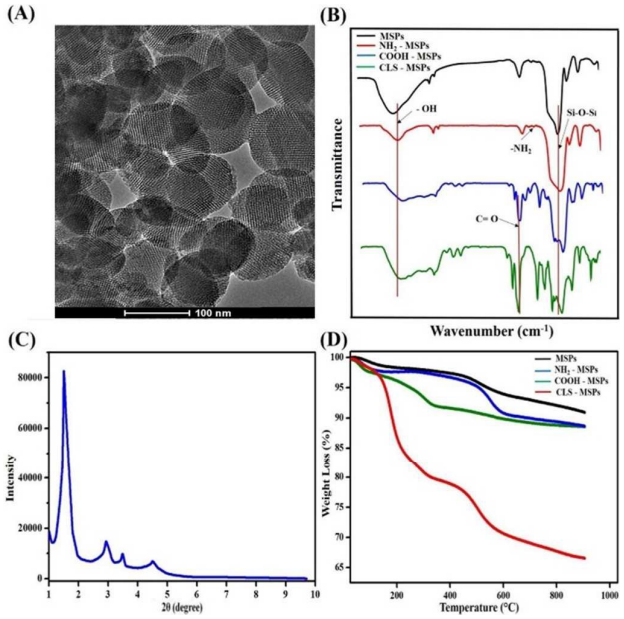

Figure 2: (A) Transmission Electron Microscope Images of MSPs; MSPs were dried at 80 ^{0}C under high vacuum for 12 hours before taking TEM images. MSPs were dispersed in ethanol and spotted on the copper gird. **(B)** FTIR Spectrum of MSPs, NH_2-MSPs, COOH-MSPs and CLS- MSPs. **(C)** XRD pattern of MSPs; specific pattern of MCM-41 type MSPs **(D)** TGA curves of MSPs, NH_2-MSPs, COOH-MSPs and CLS-MSPs. CLS-MSPs shown more weight loss than MSPs, NH_2-MSPs and COOH-MSPs.

N_2-absorption/desorption was carried by using ASAP 2020 sorptometer at 77K. N_2-adsorption/desorption isotherms of MSPs show the characteristic IV sort hysteresis ofMCM-41 type MSPs (Figure 3A). The characterized sorption steps between 0.5-0.7 relative pressures (P/P_0) suggest that nanoparticles have consistent mesoporous layers of pores throughout the surface.

The surface area of synthesized nanoparticles was measured through BET. The surface area of MSPs, NH_2-MSPs, COOH-MSPs and DOX/CLS-MSPs was about 932, 857, 694 and 486m^2/g, respectively. Pore size and pore volume of MSPs, NH_2-MSPs and COOH-MSPs nanoparticles were measured from their N_2-adsorption/desorption isotherms by using BJH methods. The pore size of MSPs, NH_2-MSPs, and COOH -MSPs was 3.64, 2.97 and 2.72 nm (Table S1), respectively; while the pore volume of MSPs, NH_2-MSPs, and COOH-MSPs was 0.92, 0.79 and 0.72 cm^3/g, respectively. Notwithstanding, the nitrogen adsorption was reduced from MSPs to COOH -MSPs but form of hysteresis loop pertained identical in all type of nanoparticles (Figure S1 A-C, supplementary information), which confirmed that pore shape was not disrupted during surface modification. However, little decrease in the pore size and pore volume of MSPs was observed after modification that might be due to conjugation of NH_2 and COOH groups inside the pores but it was not so obvious. On the other hand, no hysteresis in DOX/CLS-MSPs (Figure S1D) suggests that pores were occupied by DOX and sealed well with cellulose polymer.

The zeta potential of MSPs, NH_2- MSPs, COOH-MSPs and CLS-MSPs nanoparticles were measured by dynamic light scattering (DLS; Zeta Sizer Nano-ZS 90, Malvern InstrumentsLtd., Worcestershire, UK) equipped with a He-Ne laser (λ=633 nm) with the scattering angle of 90°. All samples were diluted with water to 0.1 mg/mL and maintained for 5 min at the designed temperature ranged from 20 to 50 °C before testing. Agilent Carry 60 UV/Visible Spectrometer was used to record the absorbance readout. Olympus FV1000 confocal microscope (Tokyo, Japan) was used to take cell images.

Stability of DOX/CLS-MSPs in physiological conditions: To improve drug efficiency, the reticence of toxic side effects of drugs is very key to anti-cancer and MDR overcoming. One of the most accepted routes is to endow drug delivery systems (DDSs) with the stimuli responsive drug release character. The most significant case is that drugs do not or barely release in normal tissues and blood (pH ~ 7.4) but can effectively release in tumor tissues, or even within cancer cells selectively to kill cancer cells (pH ~ 4.0 - 6.8). Nonetheless, several DDSs have been proposed to release drugs under in *vitro* acidified conditions of tumors; however, to effectively suppress drug release as slowly as possible in normal physiological conditions (pH ~ 7.4) is still a great task. Here, this nano DDS has achieved a desired stability under physiological conditions and stimuli responsive drug release character.

To examine the stability of DOX/CLS-MSPs under physiological conditions, MSPs and COOH-MSPs were soaked in DOX solution for 48 h separately and then COOH-MSPs were further conjugated with cellulose to give rise DOX/CLS-MSPs while DOX loaded mesoporous silica nanoparticles (DOX/MSPs) were remained as such. Then, both DOX loaded MSPs (DOX/MSPs) and DOX loaded cellulose conjugated MSPs (DOX/CLS-MSPs) were collected by centrifugation at 4000 rpm for 10 minutes and washed with water gently. Subsequently, an experiment

was conducted to observe the DOX release behaviour from DOX/ CLS-MSPs in comparison with DOX/MSPs in pH 7.4 PBS solution (pH: 7.4) at 37 °C. The drug release from cellulose conjugated DOX/CLS-MSPs was only 10.87% in contrast with DOX/MSPs where it was 75.39% (Figure 3B). It suggested that DOX/CLS-MSPs nanotherapeutics were very stable under physiological conditions (pH ~ 7.4) and drug release was well controlled by cellulose blocking the outlets of pores that avoided the premature DOX release under physiologicalcondition.

In *vitro* stimuli responsive DOX release: To explore stimuli responsive drug release from DOX/CLS-MSPs, pH and cellulase responsive DOX release experiments were performed. Acidified conditions were first used as a trigger to observe DOX release in PBS solution. DOX/CLS-MSPs were dispersed in five different pH PBS solution (pH: 4.0, 5.0, 6.0, and 7.4). DOX release was studied by absorption spectra at λ_{max}: 480 nm at different time intervals at 37 °C. pH responsive DOX release quantities from DOX/CLS-MSPs in PBS solution (pH: 4.0, 5.0, 6.0, and 7.4) were 62.61, 54.43, 45.94 and 10.51% respectively for 27 hours (Figure 3C). These results suggested that DOX loaded nanotherapeutics were well pH responsive. In acidified catalysed condition, ester linkage between COOH group of MSPs and OH group of cellulose is hydrolysed that lets the pores open to allow drug molecules to come out through diffusion. At pH 4.0 more DOX release suggests that acid catalysed hydrolysis of ester bond is more effective in higher acidic environment. Less amount of DOX release at

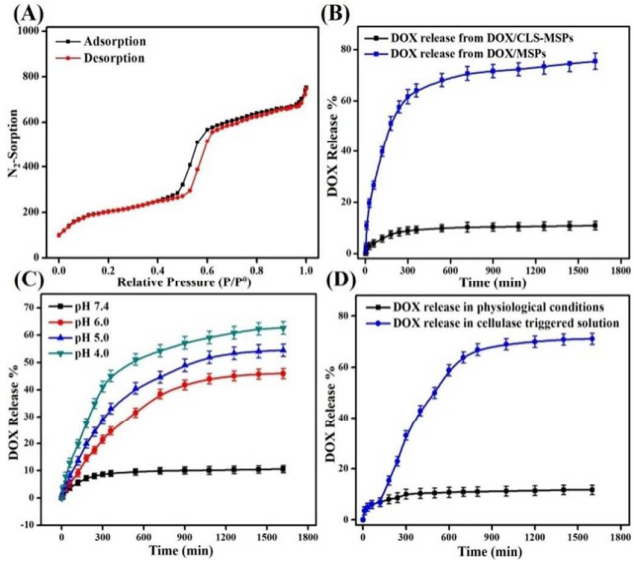

Figure 3: (A) N_2-adsorption/desorption isotherms of MSPs **(B)** Stability of DOX/CLS-MSPs under physiological conditions; DOX release from DOX/CLS-MSPs was only 10.87% in pH 7.4 PBS while in comparison the DOX release from MSPs was 75.39%. **(C)** pH triggered DOX release from DOX/CLS-MSPs in PBS solutions; DOX release in pH 4.0, 5.0, 6.0 & 7.4 PBS was 62.61, 54.43, 45.94 & 10.51%, respectively. **(D)** Cellulase triggered DOX release study; DOX release in cellulase triggered pH 7.4 PBS buffer was about 71%, triggered after two hours since the start time while in contrast only 11.19 % in non-triggered pH 7.4 PBS solution. Data in Figures (B, C & D) represents the mean ± standard deviation (n=3)

physiological conditions (pH 7.4), confirms that MSPs based nanotherapeutics were stable under these conditions to avoid premature drug release while effective in tumorous acidified conditions. We anticipated that this could be more useful to release cargo on the targeted tumors that have more acidified cellular environments.

Next in *vitro* release of DOX from DOX/CLS-MSPs was carried by using cellulase glycosidase enzyme. DOX/CLS-MSPs were dispersed in pH 7.4 PBS buffer solution and release of DOX was measured at different time intervals for two hours and then triggered with cellulase solution. A sudden increase in drug release was observed in cellulase triggered sample. DOX release extent in cellulase triggered sample (Figure 3D) was about 71% while in contrast the DOX release content in non-triggered sample was only 11.19 %. This suggests that cellulase digests the glycoside linkages of cellulose polymer molecules and converts it into glucose monomers leaving the pores of MSPs open for drug molecules to diffuse through. We anticipate that this fast drug release can be productive in cellular lysosomal/endosomal where many glycosidase enzymes are found and effective in trigger release for anticancer cargo.

Cellular uptake of DOX/CLS-MSPs nanoparticles and intracellular DOX release: To explore the intracellular accumulation advantages of cellulose conjugated MSPs nanoparticles in the biomedical fields especially in drug delivery, the intracellular behaviour of FITC labelled-DOX/CLS-MSPs nanoparticles in HepG2 tumor cells was investigated. HepG2 were seeded in a 6 well plate at the density of 5 x 10^4 cells/well on cover glass at 37 °C and 5% CO_2 in a humidified atmosphere for overnight. Medium was removed and cells were washed three times with PBS. Cells grown cover glass were then incubated with fluorescein-labelled DOX/CLS-MSPs (50 µg/mL) for different time of courses (1, 2, and 4 h) and fixed with 4% PFA solution. Images were taken by using Olympus FV1000 confocal microscope with excitation at 488 nm and emission at 525-530 nm for FITC while with excitation at 559 nm and emission at 600–700 nm for DOX. The intracellular fluorescence of DOX/CLS-MSPs nanoparticles (Figure 4) was increased in time dependent manner.

To further investigate the effects of concentration, HepG2 Cells were incubated with different doses of DOX/CLS-MSPs (25, 50, 75 and 100 µg/mL) for different time of periods (1, 2, 4, and 6h).As shown (Figure 5), intracellular florescence of DOX was increased by concentration and time dependent manner.

Cytotoxicity Assay: To explore the cytotoxicity of DOX/CLS-MSPs on tumor cells, MTT assay was performed. HepG2 cancer cells were cultured in 96 well plate overnight at 37 °C in a humidified atmosphere and 5% CO_2 condition at the initial density of 1 x 10^4 cells/well. Then culture media was removed and cells in each well were incubated with different doses of DOX/CLS-MSPs and DOX/MSPs nanoparticles (0, 25, 50, 100, 150 and 200 µg/mL) for 24 h. The cells without nanoparticles addition (0µL/mL) were considered as control. After 24 h incubation, cell were rinsed with PBS and replaced with fresh medium.

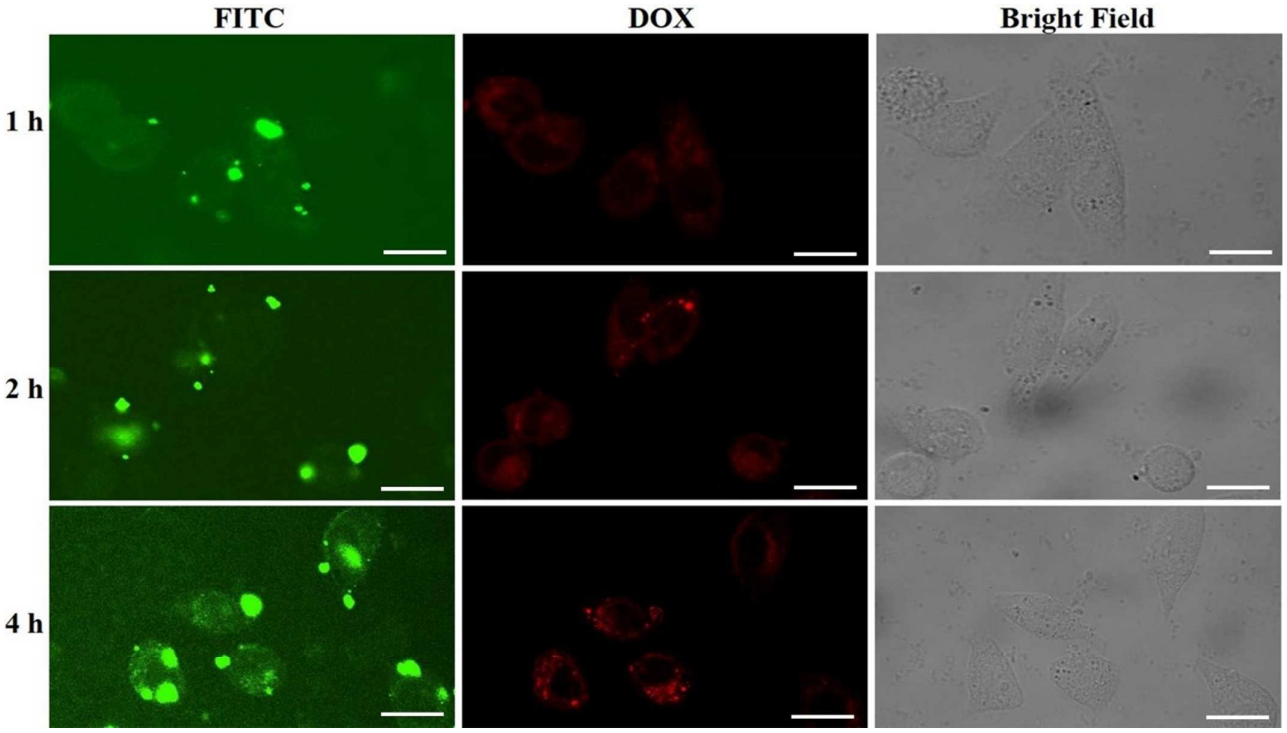

Figure 4: The intracellular accumulation of DOX/CLS-MSNPs nanoparticles and DOX release in HepG2 cell lines; HepG2 cells were treated with 50 µg/mL DOX/CLS-MSPs for different time intervals (1, 2 & 4 h). After treatment with DOX/CLS-MSPs, cells were washed three times with PBS, then fixed with 4% paraformaldehyde, and images were taken through confocal microscope. Scale bar is 60 µm.

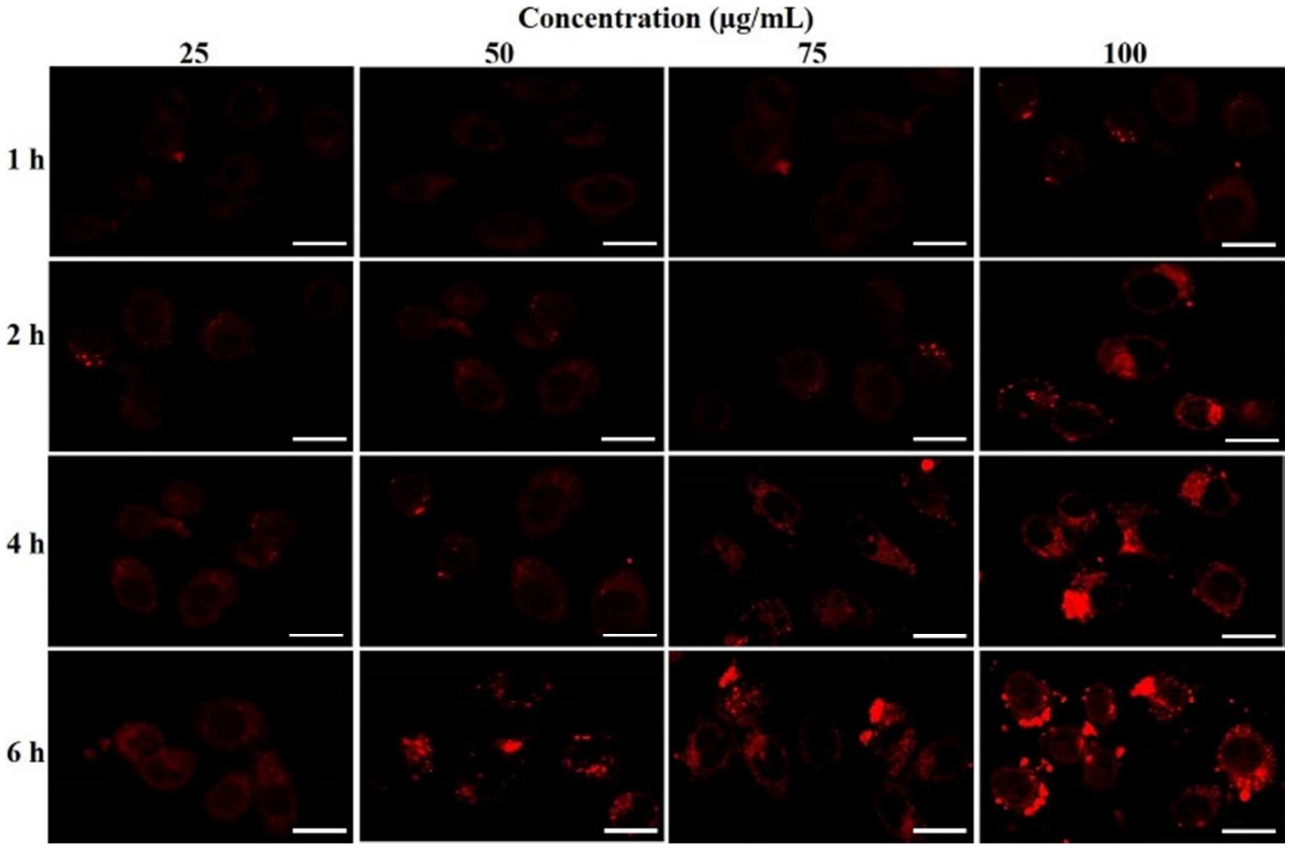

Figure 5: Effect of dose concentration of DOX/CLS-MSPs on intracellular DOX release in HepG2 cell lines; Confocal microscope images of HepG2 cells were produced after incubation with different doses of DOX/CLS-MSPs (25, 50, 75 & 100 µg/mL) for different time periods (1, 2, 4 & 6 h), Scale bar is 40 µm.

Subsequently, 20 µL of MTT solution with concentration of 3 mg/mL was added in each well and incubated for next 4 h. Culture media was then removed and 200µL of DMSO was added to solubilize the formazan crystals. After dissolution of formazan crystals, the optical density of solution was measured by absorbance readout through microplate reader at wavelength of 490 nm. Six replicates of each concentration were produced. Cell viability was standardized as percentage of the cells incubated with nanoparticles with that of control cells. DOX/CLS-MSPs were shown more cellular cytotoxicity (Figure 6) than DOX/MSPs. These results suggest that DOX/CLS-MSPs have shown more cytotoxicity and appropriate for effective doxorubicin delivery due to cationic feature of cellulose which supports the intracellular accumulation.

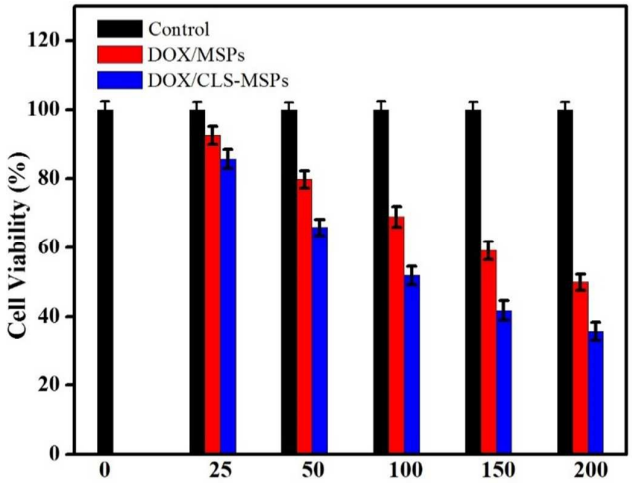

Figure 6: Cytotoxicity Assay; cellular viability of HepG2 cancer cells were determined after incubation with different doses (0, 25, 50, 100, 150 and 200µg/mL) of MSPs, DOX/CLS-MSPs and DOX/MSPs for 24 h. The untreated cells with nanoparticles were considered as control. Data shows the mean ± standard deviation (n=6).

Experimental

Materials and Reagents: Tetraethylorthosilcate (TEOS), N-cetyltrimethylammonium bromide (CTAB), 1-ethyl-3-(3-dimethylaminopropyl) carbimide. HCl (EDC) and doxorubicin were purchased from Aladdin. Succinic anhydride (SA), cellulose microcrystalline stuff, (3-aminopropyl) trimethoxysilane (APTES), N-hydroxysuccinimide (NHS), and cellulase were purchased from Sigma Aldrich. Sodium hydroxide (NaOH), 37% pure hydrochloric acid, methanol, anhydrous toluene, acetone, acetic acid and other laboratory reagents were provided by Sinopharm chemical reagents co. limited China. All chemicals were used in original form as received from the relevant manufacturing company without any further purification. Ultra nanopure distilled water (18.2MΩ) was utilized throughout practical work and in preparation of phosphate buffer solution (PBS). MTT reagent 3-(4, 5-dimethylthiazol-2-yl)-2, 5-diphenyltetrazolium bromide was provided by Sigma Aldrich.

Preparation of MSPs and their surface modification: Mesoporous silica nanoparticles (MSPs) with average diameter around 120 nm were fabricated through sol-gel method according to strategy as shown in the flow chart (Figure 1). Briefly 1.0 g of N-cetyltrimethylammonium bromide (CTAB) and 0.28 g of NaOH were dissolved in 500 mL of distilled water and then heated up to 80 ^{0}C. Followed by addition of TEOS (4 mL) drop wisely with constant magnetic stirring. Then, TEOS and NaOH mixture was stirred continuously at 80 °C for 2 h until white precipitates were formed. This was followed by centrifugation of these white precipitates at 4000 rpm for 10 minutes. Subsequently, the centrifuged residue was rinsed with excessive water and methanol then followed by air dry for 24 h. The remaining CTAB surfactant was removed by refluxing solid stuff in solution containing HCl (37%, 2 mL) and methanol (120 mL) for overnight at room temperature and followed by filtration and rinsing with copious amount of distilled water and methanol. This stuff was then dried under high vacuum (-0.01mPa) for 12 hours at 80 °C to remove remaining residual surfactant and solvent molecules entirely from the pores of silica nanoparticles.

To modify NH_2 on the surface of silica nanoparticles, 1.0 g MSPs was refluxed in a mixture containing (3-aminopropyl) trimethoxysilane (APTES), 2 mL and anhydrous dry toluene (100 mL) for 24 h. Subsequently, nanoparticles were filtered off, rinsed with excess distilled water and methanol and dried at 80 °C under high vacuum overnight. This solid stuff was ammonized or APTES modified silica nanoparticles (NH_2-MSPs).

As for fluorescein labelled mesoporous silica nanoparticle, 2.5 mg of fluorescein isothiocyanate (FITC) was treated with APTES (100 µL) in ethanol (3 mL) overnight in dark conditions. CTAB (0.45 g) was first dissolved in 200 mL of water. Sodium hydroxide (2 mL, 2M) was added to CTAB solution and then solution was heated up to 80 °C. Tetraethylorthosilicate (TEOS), 3 mL was added drop wise and then followed by the addition of APTES modified FITC solution (250 µL) with constant stirring. This mixture was allowed to stir for 2 h to give rise precipitate. Finally, the surfactant was removed by refluxing this stuff in acidified methanol solution to obtain fluorescein-labelled ammonized mesoporous silica nanoparticle.

To modify COOH group on the surface of NH_2-MSPs, 500 mg of NH_2-MSPs or FITC-labelled NH_2-MSPs were dispersed in acetone (50 mL) with constant stirring at ambient temperature for 4 hours, followed by addition of succinic anhydride (20 mL, 2 M) solution in acetone drop wisely with constant stirring and then mixture was left to stir for overnight at ambient temperature. After mixture was filtered off and residue was rinsed with copious amount of water and methanol to remove excess succinic anhydride and solvent molecules. The white residue was dried under high vacuum (-0.01mPa) again at 50 °C to remove the solvent molecules from the pores of nanoparticles completely in order to increase the drug loading efficiency of mesopores. The obtained white solid stuff was carboxylated mesoporous silica nanoparticles (COOH-MSPs).

Dissolution of cellulose and conjugation with COOH-MSPs by esterification: A new method was developed for dissolution of microcrystalline cellulose and successfully achieved cellulose (2%) solution in only 5% NaOH solution. Briefly, NaOH, 5g was dissolved in 50 mL distilled water. Subsequently, 2 g microcrystalline cellulose stuff was added in NaOH solution and stirred mechanically for few minutes. Then allowed the cellulose to swell for one hour and subsequently suspension was frozen into a solid mass by holding it at – 4°C overnight. This was followed by thawing the frozen mass at room temperature and diluting with water to 5% NaOH by adding 50 mL more water. Subsequently, stirred mechanically for few minutes and white gelatinous viscous solution of cellulose was obtained.

Esterification of COOH-MSPs with cellulose was carried between surface carboxylic group of MSPs and OH group of cellulose. Briefly, 300 mg carboxylated silica nanoparticles (COOH-MSPs) were refluxed in acetate buffer (50 mL, pH: 5.0) solution and followed with the addition of EDC/NHS mixture (EDC= 0.2M, NHS= 0.2 M) in acetate buffer (25 mL, pH: 5.0) to activate the carboxylic group of silica nanoparticles. Then, the mixture was allowed to settle for 4 h to attain stable suspension at ambient temperature and followed by addition of cellulose solution (10 mL, 2% in 5% NaOH solution) drop wise and then mixture was stirred overnight at ambient temperature. After overnight stirring, cellulose conjugated mesoporous silica nanoparticles (CLS-MSPs) were centrifuged, filtered off, rinsed with copious distilled water to remove the excessive cellulose and remaining solvent then this stuff was dried at 45 °C for overnight and then characterized with different techniques.

Doxorubicin loading and surface conjugating with cellulose: Doxorubicin (5 mg) was dissolved in 5 mL distilled water then diluted to desired level to measure the absorbance to note the initial concentration through absorbance. 100 mg carboxylated mesoporous silica nanoparticles (COOH-MSPs) were dispersed in the DOX solution and then nanoparticles was allowed to soak maximum drug molecules with constant stirring for next 48 hours. Subsequently, acetate buffer solution (10 mL, pH 5.0) containing mixture of EDC and NHS (EDC: 0.2 M; NHS: 0.2 M) was added and then suspension allowed to settle at ambient temperature for next 4 h. Followed by addition of 10 mL 2% cellulose solution drop wisely with constant stirring and then again suspension was stirred for next 6 hours at ambient temperature. Finally, cellulose conjugated DOX loaded mesoporous silica nanoparticles (DOX/CLS-MSPs) were centrifuged, rinsed with distilled water gently to remove excess cellulose content and surface drug molecules. The drug loading capacity of silica nanoparticles was determined through the difference in the concentrations of initial and left drug in solution by using UV/Vis absorbance readout at λ_{max}: 480nm. The DOX loading capacity of MSPs was about 42µmol/g.

DOX loading Capacity (DLC) in MSNs-COOH was calculated by UV–vis spectroscopy[24d]. DLC of DOX in MSNs-COOH was expressed as % of total DOX added according to equation

$$\text{DOX loading Capacity (\%)} = \frac{\text{Amount of DOX in MSPs}-\text{COOH}}{\text{Amount of total DOX added}} \times 100$$

The amount of DOX released from DOX/CLS-MSPs was calculated as;

$$\text{DOX release (\%)} = \frac{\text{DOX released from DOX/CLS}-\text{MSPs}}{\text{Total DOX loaded in DOX/CLS}-\text{MSPs}} \times 100$$

To produce the FITC-labelled DOX/CLS-MSPs, the above procedure repeated with FITC-labelled COOH-MSPs nanoparticles.

Stimuli triggered DOX release: For pH triggered DOX release, 5 mg of DOX/ CLS-MSPs were suspended in 1 mL of each of four different pH PBS solutions (7.4, 6.0, 5.0, & 4.0) in dialysis membrane bags (MWCO=5300) and then bag was immersed in 5 mL of similar pH buffer and stirred at 37 °C. Subsequently, the aliquots were taken from the each PBS solution in different time intervals and DOX release was noted through absorbance on UV/Visible spectrometer at λ_{max}: 480nm. The DOX release from DOX/CLS-MSPs was studied for 27 hours. This experiment was repeated three times for each pH condition to produce three replicates.

For cellulase triggered DOX release study, 5 mg of DOX/ CLS-MSPs were suspended in 1 mL of PBS (pH: 7.4) in each of two dialysis membrane bags and then each bag was immersed in 5 mL of similar pH PBS in two different tubes and stirred at 37 °C. DOX release was observed for different time periods till 2 hours and then one sample was triggered by adding 1 mL cellulase solution while other sample was continued with same condition. Then again aliquots were taken from the each solution at different time intervals and DOX release in cellulase triggered PBS solution and non-triggered PBS solution was observed for next 27 hours. This experiment was also repeated three times to produce three replicates.

Cell Culture and confocal microscope magnification: The human cancer cell lines (HepG2cells) were provided by Type Culture Collection of the Chinese Academy of Sciences (Shanghai, China). The cells were cultured in the DMEM culture medium (Gibco, New York, USA) containing 10% fetal bovine serum, 100U/mL penicillin and 100µg/mL streptomycin. All cells were maintained at 37 °C in a humidified atmosphere and 5 % CO_2 incubator. After every 2 days, culture media was removed and cells were cultured in fresh medium.

For confocal microscope magnification, HepG2 cells were seeded on cover glass at a density of 5×10^4 cells/well in 6 - well plate overnight. Medium was then removed and cells were incubated with 50µg/mL of DOX/CLS-MSPs for different time intervals (1, 2 and 4 h). After incubation, cells were washed with PBS, fixed with 4% paraformaldehyde and again washed with PBS. The cover glass was then mounted on the slide. Confocal Images were taken by Olympus FV1000 high resolution confocal microscope (Tokyo, Japan) with excitation

at 488 nm and emission at 525-530 nm for FITC and with excitation at 559 nm and emission at 600-700 nm for DOX. To explore the effect of DOX/CLS-MSPs concentration, cells were seeded on a cover glass in a 6 well plate and then incubated with different doses of DOX/CLS-MSPs nanoparticles (25, 50, 75 and 100 μg/mL) for different time periods (1, 2, 4 and 6 h).

Conclusion

In summary, we have successfully fabricated fluorescent DOX/CLS-MSPs nanotherapeutics by simple sol-gel strategy. Esterification has been carried out between cellulose polymer and carboxylated MSPs to conjugate the cellulose on surface of MSPs to control doxorubicin release under physiological conditions. We have effectively accomplished pH and cellulase triggered in *vitro* doxorubicin release. Intracellular accumulation of DOX/CLS-MSPs and DOX release in HepG2 cancer cells have been observed through confocal microscope magnification. We have conducted MTT assay to observe cell cytotoxicity of DOX/CLS-MSPs on HepG2 tumor cells. The brilliant cytotoxicity toward tumor cells and effective drug release of DOX/CLS-MSPs nanotherapeutics drew attention to their vast biomedical applications especially in *vivo* sustainable anticancer drug delivery in future chemotherapy. We anticipate that this attempt might be productive for cancer treatment in future perspective.

Acknowledgements

This research is supported by National Basic Research Program of China (973 program, 2015CB932600, and 2013CB933000), National Natural Science Foundation of China (21375042, 21405054, 21525523, and 21574048) and 1000 Young Talent (to Fan Xia).

Notes

Authors declare no competing financial interest.

References

1 (a) M. M. Gottesman, *Annual Review of Medicine*, 2002, **53**, 615-627; (b) G. I. Evan and K. H. Vousden, *Nature*, 2001, **411**, 342-348; (c) W. Tai, R. Mo, Y. Lu, T. Jiang and Z. Gu, *Biomaterials*, 2014, **35**, 7194-7203; (d) C. Ju, R. Mo, J. Xue, L. Zhang, Z. Zhao, L. Xue, Q. Ping and C. Zhang, *Angew. Chem. Int. Ed.*, 2014.

2 (a) P. M. Winter, S. D. Caruthers, A. Kassner, T. D. Harris, L. K. Chinen, J. S. Allen, E. K. Lacy, H. Zhang, J. D. Robertson, S. A. Wickline and G. M. Lanza, *Cancer Research*, 2003, **63**, 5838-5843; (b) T. Wang, L. Zhang, Z. Su, C. Wang, Y. Liao and Q. Fu, *ACS Applied Materials & Interfaces*, 2011, **3**, 2479-2486; (c) E. Tahara, H. Ito, K. Nakagami, F. Shimamoto, M. Yamamoto and K. Sumii, *Cancer*, 1982, **49**, 1904-1915.

3 (a) J. Xie, G. Liu, H. S. Eden, H. Ai and X. Chen, *Accounts Chem. Res.*, 2011, **44**, 883-892; (b) S. Dhar, F. X. Gu, R. Langer, O. C. Farokhzad and S. J. Lippard, *Proc. Natl. Acad. Sci.,* 2008, **105**, 17356-17361; (c) M. Ferrari, *Nat Rev Cancer*, 2005, **5**, 161-171.

4 (a) D. Schmaljohann, *Advanced Drug Delivery Reviews*, 2006, **58**, 1655-1670; (b) H. Meng, M. Liong, T. Xia, Z. Li, Z. Ji, J. I. Zink and A. E. Nel, *ACS Nano*, 2010, **4**, 4539-4550; (c) A. L. Martin, L. M. Bernas, B. K. Rutt, P. J. Foster and E. R. Gillies, *Bioconjugate Chemistry*, 2008, **19**, 2375-2384.

5 (a) P. Yang, S. Gai and J. Lin, *Chem. Soc. Rev.*, 2012, **41**, 3679-3698; (b) Q. Quan, J. Xie, H. Gao, M. Yang, F. Zhang, G. Liu, X. Lin, A. Wang, H. S. Eden, S. Lee, G. Zhang and X. Chen, *Molecular Pharmaceutics*, 2011, **8**, 1669-1676; (c) P. Gupta, K. Vermani and S. Garg, *Drug Discovery Today*, 2002, **7**, 569-579.

6 (a) B.S. Kim, S. W. Park and P. T. Hammond, *ACS Nano*, 2008, **2**, 386-392; (b) W. T. Al-Jamal and K. Kostarelos, *Accounts Chem. Res.*, 2011, **44**, 1094-1104; (c) M. M. Boyle, R. A. Smaldone, A. C. Whalley, M. W. Ambrogio, Y. Y. Botros and J. F. Stoddart, *Chem. Science*, 2011, **2**, 204-210.

7 (a) H. T. T. Duong, C. P. Marquis, M. Whittaker, T. P. Davis and C. Boyer, *Macromolecules*, 2011, **44**, 8008-8019; (b) G. F. Paciotti, D. G. I. Kingston and L. Tamarkin, Drug Development Research, 2006, **67**, 47-54; (c) Y. Wang, Y. Yan, J. Cui, L. Hosta-Rigau, J. K. Heath, E. C. Nice and F. Caruso, *Advanced Materials*, 2010, **22**, 4293-4297.

8 (a) Y. Malam, M. Loizidou and A. M. Seifalian, *Trends in Pharmacological Sciences*, 2009, **30**, 592-599; (b) K. K. Cotí, M. E. Belowich, M. Liong, M. W. Ambrogio, Y. A. Lau, H. A. Khatib, J. I. Zink, N. M. Khashab and J. F. Stoddart, *Nanoscale*, 2009, **1**, 16-39; (c) Q. He and J. Shi, *J. Mater. Chem.*, 2011, **21**, 5845-5855.

9 (a) K. Cho, X. Wang, S. Nie, Z. Chen and D. M. Shin, *Clinical Cancer Research*, 2008, **14**, 1310-1316; (b) Z. Tao, *RSC Advances*, 2014, **4**, 18961-18980; (c) A. L. Parry, N. A. Clemson, J. Ellis, S. S. R. Bernhard, B. G. Davis and N. R. Cameron, *J. Am. Chem. Soc.*, 2013, **135**, 9362-9365.

10 (a) M. Liong, J. Lu, M. Kovochich, T. Xia, S. G. Ruehm, A. E. Nel, F. Tamanoi and J. I. Zink, *ACS Nano*, 2008, **2**, 889-896; (b) Y. Sasaki and K. Akiyoshi, *The Chemical Record*, 2010, **10**, 366-376; (c) W. J. Rieter, K. M. Pott, K. M. L. Taylor and W. Lin, *J. Am. Chem. Soc.*, 2008, **130**, 11584-11585.

11 (a) Y. Shen, E. Jin, B. Zhang, C. J. Murphy, M. Sui, J. Zhao, J. Wang, J. Tang, M. Fan, E. Van Kirk and W. J. Murdoch, *J. Am. Chem. Soc.*, 2010, **132**, 4259-4265; (b) Y. S. Lin and C. L. Haynes, *Chem. Mater.*, 2009, **21**, 3979-3986; (c) K. Cho, X. Wang, S. Nie, Z. Chen and D. M. Shin, *Clinical Cancer Research*, 2008, **14**, 1310-1316.

12 (a) T. Lebold, C. Jung, J. Michaelis and C. Bräuchle, *Nano Letters*, 2009, **9**, 2877-2883; (b)L. Pan, Q. He, J. Liu, Y. Chen, M. Ma, L. Zhang and J. Shi, *J. Am. Chem. Soc.*, 2012, **134**, 5722-5725; (c) J. L. Vivero-Escoto, I. I. Slowing, C.W. Wu and V. S. Y. Lin, *J. Am. Chem. Soc.*, 2009, **131**, 3462-3463.

13 (a) F. Muhammad, M. Guo, W. Qi, F. Sun, A. Wang, Y. Guo and G. Zhu, *J. Am. Chem. Soc.*, 2011, **133**, 8778-8781; (b) J. Guo, W. Yang, C. Wang, J. He and J. Chen, *Chem. Mater.*, 2006, **18**, 5554-5562; (c) J. E. Lee, N. Lee, H. Kim, J. Kim, S. H. Choi, J. H. Kim, T. Kim, I. C. Song, S. P. Park, W. K. Moon and T. Hyeon, *J. Am. Chem. Soc.*, 2009, **132**, 552-557.

14 (a) J. Lu, M. Liong, Z. Li, J. I. Zink and F. Tamanoi, *Small*, 2010, **6**, 1794-1805; (b) J. Lu, M. Liong, J. I. Zink and F. Tamanoi,

Small, 2007, **3**, 1341-1346; (c) B. G. Trewyn, I. I. Slowing, S. Giri, H.-T. Chen and V. S. Y. Lin, *Accounts Chem. Res.*, 2007, **40**, 846-853.

15 (a) L. Cheng, C. Wang, L. Feng, K. Yang and Z. Liu, *Chem. Rev.*, 2014, **114**, 10869-10939; (b) H. Meng, M. Xue, T. Xia, Y. L. Zhao, F. Tamanoi, J. F. Stoddart, J. I. Zink and A. E. Nel, *J. Am. Chem. Soc.*, 2010, **132**, 12690-12697; (c) L.S. Wang, L. C. Wu, S. Y. Lu, L. L. Chang, I. T. Teng, C. M. Yang and J. A. Ho, *ACS Nano*, 2010, **4**, 4371-4379.

16 (a) C. L. Zhu, C. H. Lu, X. Y. Song, H. H. Yang and X. R. Wang, *J. Am. Chem. Soc.*, 2011, **133**, 1278-1281; (b) N. Singh, A. Karambelkar, L. Gu, K. Lin, J. S. Miller, C. S. Chen, M. J. Sailor and S. N. Bhatia, *J. Am. Chem. Soc.*, 2011, **133**, 19582-19585; (c) L. Du, S. Liao, H. A. Khatib, J. F. Stoddart and J. I. Zink, *J. Am. Chem. Soc.*, 2009, **131**, 15136-15142.

17 (a) J. C. Doadrio, E. M. B. Sousa, I. Izquierdo-Barba, A. L. Doadrio, J. Perez-Pariente and M. Vallet-Regi, *J. Mater. Chem.*, 2006, **16**, 462-466; (b) M. W. Ambrogio, C. R. Thomas, Y.-L. Zhao, J. I. Zink and J. F. Stoddart, *Accounts Chem. Res.*, 2011, **44**, 903-913; (c) D. Tarn, C. E. Ashley, M. Xue, E. C. Carnes, J. I. Zink and C. J. Brinker, *Accounts Chem. Res.*, 2013, **46**, 792-801.

18 (a) E. Climent, A. Bernardos, R. Martínez-Máñez, A. Maquieira, M. D. Marcos, N. Pastor-Navarro, R. Puchades, F. Sancenón, J. Soto and P. Amorós, *J. Am. Chem. Soc.*, 2009, **131**, 14075-14080; (b) Y. Gao, Y. Chen, X. Ji, X. He, Q. Yin, Z. Zhang, J. Shi and Y. Li, *ACS Nano*, 2011, **5**, 9788-9798.

19 (a) C. Park, K. Oh, S. C. Lee and C. Kim, *Angew. Chem. Int. Ed.*, 2007, **46**, 1455-1457; (b) A. Hakeem, R. Duan, F. Zahid, C. Dong, B. Wang, F. Hong, X. Ou, Y. Jia and F. Xia, *Chem. Commun.*, 2014; (c) T. Suteewong, H. Sai, R. Cohen, S. Wang, M. Bradbury, B. Baird, S. M. Gruner and U. Wiesner, *J. Am. Chem. Soc.*, 2010, **133**, 172-175.

20 (a) Y. Zhao, B. G. Trewyn, I. I. Slowing and V. S. Y. Lin, *J. Am. Chem. Soc.*, 2009, **131**, 8398-8400; (b) Z. Luo, K. Cai, Y. Hu, L. Zhao, P. Liu, L. Duan and W. Yang, *Angew. Chem. Int. Ed.*, 2011, **50**, 640-643; (c) C.Y. Lai, B. G. Trewyn, D. M. Jeftinija, K. Jeftinija, S. Xu, S. Jeftinija and V. S. Y. Lin, *J. Am. Chem. Soc.*, 2003, **125**, 4451-4459.

21 (a) R. Duan, B. Wang, F. Hong, T. Zhang, Y. Jia, J. Huang, A. Hakeem, N. Liu, X. Lou and F. Xia, *Nanoscale*, 2015, **7**, 5719-5725. (b) Y. Jia, B. Wei, R. Duan, Y. Zhang, B. Wang, A. Hakeem, N. Liu, X. Ou, S. Xu, Z. Chen, X. Lou and F. Xia, *Sci. Rep.*, 2014, **4**. (c) T. Zhang, C. Shang, R. Duan, A. Hakeem, Z. Zhang, X. Lou and F. Xia, *Analyst*, 2015, **140**, 2023-2028.

22 (a) Z. Zou, D. He, X. He, K. Wang, X. Yang, Z. Qing and Q. Zhou, *Langmuir*, 2013, **29**, 12804-12810; (b) C. Chen, J. Geng, F. Pu, X. Yang, J. Ren and X. Qu, *Angew. Chem. Int. Ed.*, 2011, **50**, 882-886; (c) L. Yuan, Q. Tang, D. Yang, J. Z. Zhang, F. Zhang and J. Hu, *J. Phys. Chem. C*, 2011, **115**, 9926-9932; (d) Y. Cui, H.Dong, X. Cai, D. Wang, Y. Li, *ACS applied materials & interfaces* 2012, ***4***, 3177-3183.